PROCEEDINGS of the
24th International Congress on Acoustics

October 24 to 28, 2022 in Gyeongju, Korea

# A new strategy of designing micro vortex generators to mitigate tonal noise generation from voluteless centrifugal fan

Martin OTTERSTEN[1,2]; Hua-Dong YAO[2]; Lars DAVIDSON[2]

[1] Division of Fluid Dynamics, Department of Mechanics and Maritime, Chalmers University of Technology, Gothenburg, Sweden

[2] Swegon Operations AB, Gothenburg, Sweden

## ABSTRACT

Low-speed voluteless centrifugal fans are typically used in ventilation systems. The negative side of the fans is noise, particularly tonal noise of which the dominant tone is at the blade passing frequency ($BPF$). One of the important noise contributors is the gap between the rotating shroud and the stationary inlet duct. Previous studies have shown that the flow passing through the gap causes turbulence that interacts with the blade leading edge (BLE), rendering surface pressure fluctuations that are the tonal noise sources at $BPF$. In this study, a method of assembling micro vortex generators (MVGs) to control the turbulence for voluteless centrifugal fans is proposed for the first time. The assembling is made in two different ways: 14 add-ons on the shroud surface at the gap, and 7 ones on the BLE surface near the shroud. The effects of the MVGs are investigated using the hybrid computational aeroacoustics method, which couples the improved delayed detached eddy simulation method with the Ffowcs Williams and Hawkings acoustic analogy. Our simulations show that the MVGs are effective to control the turbulence and mitigate the tonal noise. The assembled array of 7 MVGs achieves more reduction of the tonal noise than the 14-MVGs array.

Keywords: Tonal noise, Micro vortex generators, Computational aeroacoustics

## 1. INTRODUCTION

Today most people spend the majority of their time indoors. The indoor environmental quality (IEQ) has become more and more important. When considering IEQ we usually think about temperature, $CO_2$ level, and humidity. However, it has been noticed that sound quality is an important factor for good comfort in the indoor environment (1, 2).

Although the internal noise from heating, ventilation, and air conditioning (HVAC) systems is difficult to isolate, low-speed centrifugal fans installed in the HVAC systems are known as dominant noise contributors. Nowadays a HVAC system is usually driven by a voluteless centrifugal fan, for which a gap (i.e., a clearance) is designed between the rotating fan front shroud and the stationary inlet duct. The pressure difference between the inner and outer sides of the fan drives air to pass through the gap.

There are some previous studies on voluteless centrifugal fans. Both simulations and experiments were conducted in (3), and it was found that the tonal noise at the blade passing frequency ($BPF$) is generated from a helical unsteady inlet vortex that interacts with the rotating blades near the fan backplate. Another cause is inflow distortion, which leads to flow separation at the blade root near the backplate (4). In a recent study (5), the present authors found that dominate tones at frequencies associated with the $BPF$ are related to surface pressure fluctuations at the blade leading edge (BLE). The high surface pressure fluctuations are caused when turbulence stemming from the gap flow interacts with the BLE close to the shroud.

Micro vortex generators (MVGs) are frequently used to control flow separation (6). They create vortices that energize the boundary layer and delay separation. As found in a numerical study on wind turbines (7), the aerodynamic noise due to trailing edge turbulence is reduced when vortex generators

[1] Martin.ottersten@chalmers.se

are added. In this paper, it is the first time to propose designing MVGs for centrifugal voluteless fans. Since the turbulence of this type of fans has different characteristics from wind turbines, it is of interest to address whether MVGs are also effective for the fans.

This study aims to investigate how the tonal noise at the $BPF$ is affected when MVGs are added on the centrifugal fan. For the purpose of comparison, the reference fan without MVGs is the same as that in the previous study (5). Two fans are constructed by adding MVGs at different locations onto the reference fan. The flows in the current study are simulated using a hybrid method of the improved delayed detached eddy simulation (IDDES) (8) and the Ffowcs Williams and Hawkings (FW-H) equation (9). The IDDES is used in the flow simulation, and the FW-H is used for the noise prediction.

## 2. Configuration

The baseline fan (Case I) and the two modified fans with different MVGs arrangements (Case II and Case III) are illustrated in Figure 1. Case I is the same fan as the one studied in (5). The fan blades, shroud, and backplate are the same for all cases. This fan contains 7 blades, and the clearance (i.e., the inlet gap) colored in yellow in the figure is located between the stationary inlet duct and the rotating shroud. Case II has 14 MVGs placed on the shroud at the gap location, the size and location of the MVGs are displayed in Figure 1b. Case III has one MVG on each blade, located at the BLE close to the shroud, the size and location of the MVGs are shown in Figure 1c. As shown in Figure 1a, the fan and inlet duct are positioned within a downstream duct, and the inlet duct is connected to an upstream duct. This simple geometry layout is designed for the numerical simulations. This simplification reduces the geometry complexity but retains the principal flow and acoustic characteristics. The fan parameters are listed in Table 1.

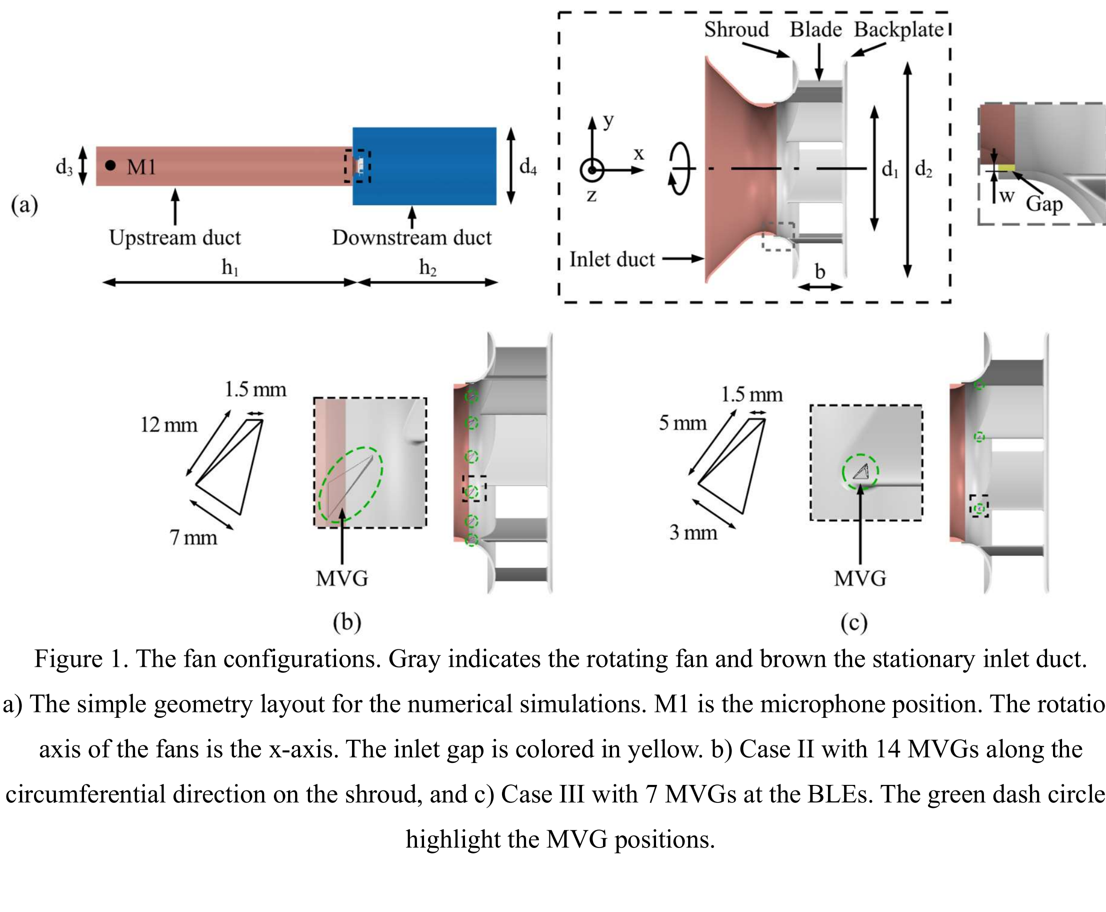


Figure 1. The fan configurations. Gray indicates the rotating fan and brown the stationary inlet duct. a) The simple geometry layout for the numerical simulations. M1 is the microphone position. The rotation axis of the fans is the x-axis. The inlet gap is colored in yellow. b) Case II with 14 MVGs along the circumferential direction on the shroud, and c) Case III with 7 MVGs at the BLEs. The green dash circles highlight the MVG positions.

Table 1. The fan parameters

| $d_1$ | $d_2$ | $d_3$ | $d_4$ | b | $h_1$ | $h_2$ | W |
|---|---|---|---|---|---|---|---|
| 0.165 m | 0.268 m | 0.6 m | 1.1 m | 0.053 m | 4.0 m | 2.3 m | 1.5 mm |

The fan rotation speed is 2800 rpm. Given that the fan has seven blades, the $BPF$ is 327 Hz, and the first harmonics $BPF_1$ is 653 Hz. The operation point is the same as in (5), where the mass flow rate was set to 0.467 kg/s and that gave a pressure rise of 270 Pa for Case I.

## 3. Numerical methodology

### 3.1 CFD method

The air is considered as an ideal gas. The flow is compressible. A finite volume method is utilized to discretize the continuity, momentum, and energy equations. The method employs a segregated flow solver accomplished with the Semi-Implicit Method for Pressure-Linked Equations (SIMPLE) algorithm. All simulations are performed using the commercial software STAR-CCM+ (10). The turbulence is simulated using the IDDES (11) that is combined with the k-ω SST turbulence model. This setup has been tested in several studies on rotating machinery (12, 13).

### 3.2 FW-H equation

A hybrid approach is adopted to predict the noise generated from the flow. In this approach, the IDDES is coupled with Formulation 1A of Farassat (14). The ambient air density is set to $\rho_0 = 1.225\ \mathrm{kg/m^3}$, and the speed of sound $c_0 = 340$ m/s.

According to Neise (15), the fan noise generation at low Mach numbers is dominated by dipole noise sources that are derived based on the FW-H equation. Hence, the noise prediction in this study considers only an impermeable integral surface for Formulation 1A. The integral surface consists of the fan blades, shroud, and backplate (see Figure 1), while the upstream and downstream ducts, as well as the fan inlet duct, are neglected. In other words, the acoustic reflection from the duct walls is neglected (16). This treatment is proposed given the fact that the acoustic reflection do not change the total power and frequency of the tonal noise, although it influences the sound intensity level because of the changed surface area of radiation. Therefore, the general trend of noise levels is still valid when the reflection is excluded in the analysis.

### 3.3 Numerical settings

The entire computational domain is divided into stationary and rotating parts. The meshes of the stationary and rotary meshes are not conformable at the interfaces between them. The flux convergence of the interpolation at the interface between the two meshes has been validated in (16).

The under-relaxation factors for the velocity and pressure in the segregated flow solver are set to 0.7 and 0.4, respectively. The under-relaxation factor for the turbulence equations is 0.7.

The mass-flow boundary condition is set at the inlet with a uniform velocity distribution. The modeled turbulence intensity is set to $I = 4\%$ according to $I = 0.16(R_e)^{-1/8}$ (10). The modeled turbulence length scale, $\ell$, is set to $0.05\ \mathrm{m}$ based on $\ell = 0.7 d_3$ where $d_3$ is the upstream duct diameter. The pressure boundary condition is set at the outlet with the static pressure of 0 Pa, and the reference pressure, $p_{ref}$=101325 Pa, defined in the ambient air. The no-slip boundary condition is specified on all walls.

The time step is set to $\Delta t = 2.0 \times 10^{-5}$ s, leading to a maximum convective Courant number of around 10 in the computational domain. This value fulfills the numerical stability required for the implicit time-marching method. The maximum number of inner iterations per time step is set to 12.

The sampling period of the noise is 0.3 s for all cases, which includes 14 fan revolutions. This leads to a frequency resolution of around 3 Hz. The FFT for the spectral calculation of sound pressure level (SPL) employs the von Hann window, where 3000 samples are chosen per signal section. The signal sections do not overlap each other.

Three cut planes (Planes 1-3) across the fan are specified to observe the flow quantities in the analysis and are shown in Figure 2. The green line is a monitoring line positioned at the BLE.

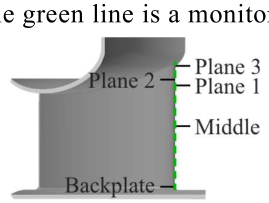


Figure 2. The cut planes for observing the flow variables. Green line is the monitoring line at the BLE.

## 4. Mesh

We adopt the same mesh generation strategy that was developed and evaluated in (5), where the fan is the same as Case I. A polyhedral mesh generation method was used to produce prism layers near the walls and polyhedral cells in the rest of the computation domain. The use of polyhedral cells for turbomachines has been demonstrated in (16, 17). The mesh parameters are listed in Table 2. The growth rate is set to 1.05, as suggested in (18). According to the guidelines of the mesh generation proposed in (5), a local refinement has to be made in the region from the gap to the BLE, and the region along the joint connection of the blade and the shroud, illustrated in **Fel! Hittar inte referenskälla.**.

Table 2. The mesh parameters

| | Case I | Case II | Case III |
|---|---|---|---|
| Total number of cells | $52 \times 10^6$ | $73 \times 10^6$ | $61 \times 10^6$ |
| Number of cells in the rotating zone | $41.9 \times 10^6$ | $63.2 \times 10^6$ | $50.9 \times 10^6$ |
| Maximum $\Delta y^+$ near blade walls | 0.73 | 0.73 | 0.73 |
| Cell growth ratio | 1.05 | 1.05 | 1.05 |

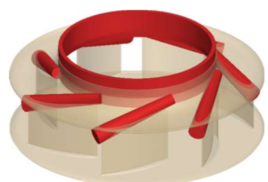

Figure 3. Mesh refinement regions (red) at the inlet gap and blades top region.

## 5. Results and discussion

### 5.1 Fan performance comparison

The static pressure excluding the reference pressure ($p_{ref} = 101325$ Pa) is displayed along the axial symmetric line for the three cases in Figure 4. All cases show similar pressure amplitudes in the upstream duct of the fan, while differences are seen downstream. Case I has the highest pressure and Case III has the lowest. Since the assembled MVGs are the only modifications amongst the fans, these add-ons are deduced to account for the differences in the pressure rise downstream of the fan.

Important physical quantities describing the fan performance are the time-averaged static pressure rise $\Delta\bar{p}$, which is between the fan inlet and outlet, and the time-averaged fan torque $\bar{M}$. These two quantities, as well as the designed mass flow rate $\bar{Q}$, are listed for all cases in **Fel! Hittar inte referenskälla.**. The fan torque increases and the static pressure rise decreases for Cases II and III compared with Case I.

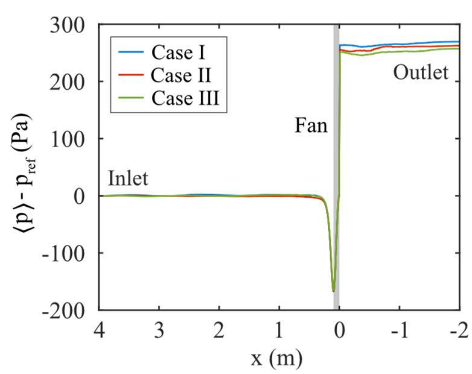


Figure 4. The pressure along the axial axis of the fan across the computational domain. Here x = −2 corresponds to the location near the outlet and x = 4 near the inlet. The fan location is marked out with the

grey zone.

Table 3. Time-averaged performance parameters of the fan

| | $\Delta\bar{p}$ (Pa) | $\bar{M}$ (N·m) | $\bar{Q}$ (kg/s) |
|---|---|---|---|
| Case I | 268 | 1.13 | 0.36 |
| Case II | 263 | 1.16 | 0.36 |
| Case III | 257 | 1.16 | 0.36 |

### 5.2 Comparison of surface pressure fluctuations

The root mean square (RMS) pressures at a monitoring line along the BLE are illustrated for all cases in Figure 5a. Here Plane 3 is in front of the BLE. The detailed information of the plane positions is referred to (5). The line follows the blade rotation, and the surface pressure is monitored during 12 fan revolutions. The same decaying tendency of the RMS pressures is observed for all three cases. At the position of the intersection between the shroud and the BLE (Plane 3), all cases present the highest RMS pressure. When the distance to the shroud increases, the RMS pressure decays to the middle of the blade span. Due to the MVGs, local differences exist between these cases. From Plane 3 to Plane 2, Case I is largest, and Case III is lowest. From Plane 1 to the backplate, Cases I and III are nearly the same. And Case II is smaller than the other cases from the blade middle span to the backplate.

The time-averaged surface pressures at the BLE are shown at different positions for all cases in Figure 4b. The maximum values in all cases occur at the shroud (Plane 3), whereas at the backplate the values are negative. The amplitudes of the maximum and minimum pressure, indicated by error bars in the figure, are largest at Plane 3. They decay when the distance from the inlet gap increases, which is a general trend for all cases. At Plane 3, Case I has the highest amplitude and Case III the lowest. At Plane 2 the maximum positive fluctuations are larger than the magnitude of the negative ones, and it is the same for all cases. Case II has the highest amplitude at the backplate. It is clear that Case III has the smallest pressure fluctuations at the BLE.

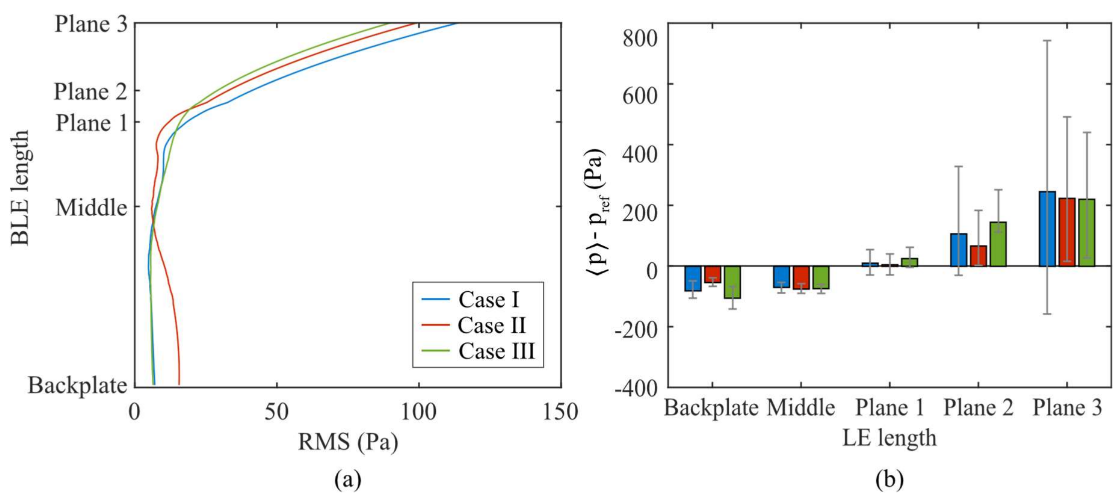


Figure 5. a) The RMS of the pressure fluctuations for 12 fan revolutions, on one blade at the monitoring line; b) the time-average pressure, where the error bars indicate the minimum and maximum pressure.

The contours of vorticity magnitudes $\|\vec{\omega}\|$ in Planes 1, 2, and 3 are shown for all cases in Figure 6. Regions with large vorticity magnitudes are detected at all planes. The area of the large vorticity is largest in Case I, and smallest in Case III. These regions move along the shroud and interact with the BLE. According to (5), surface pressure fluctuations are caused in the physical process that turbulent vortices stemming from the fan inlet gap interact with the BLE close to the shroud.

Furthermore, it is clear for all cases that the vorticity magnitudes decrease as the distance to the inlet gap increases, namely, from Plane 3 to Plane 1. This phenomenon agrees with the RMS pressure and time-averaged pressure in Figure 5. The vorticity magnitudes are effectively reduced by Case III. Correspondingly, the RMS and time-averaged pressure are reduced.

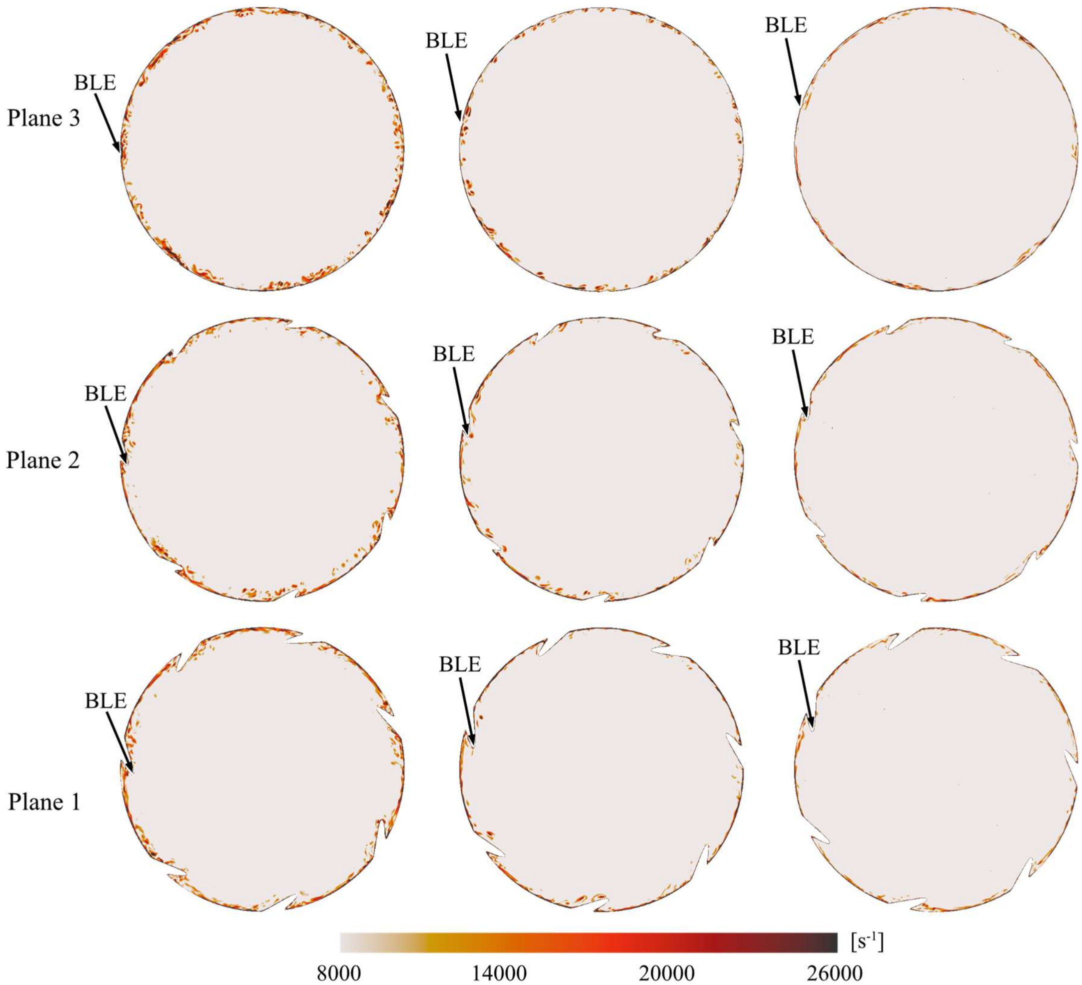

Figure 6. Instantaneous vorticity magnitudes near the shroud are visualized in Planes 1, 2, and 3; a) Case I, b) Case II, and c) Case III.

## 5.3 Spectral analysis of tonal noise sources

In the previous study of Case I (5), the predicted SPL upstream and downstream of the fan were compared with experiments. It was shown that the predicted tonal noise at $BPF$ and its first harmonic frequency, $BPF_1$ had closer agreement upstream (M1) of the fan. Hence, the same microphone position (M1) is applied to analyze the noise from the fans in this paper. As displayed in Figure 7, the noise spectra around $BPF$ and $BPF_1$ are compared. At both frequencies, the tonal peaks decrease with the rank of Case I, Case II, and Case III. This trend agrees with the results in Figures 5 and 6.

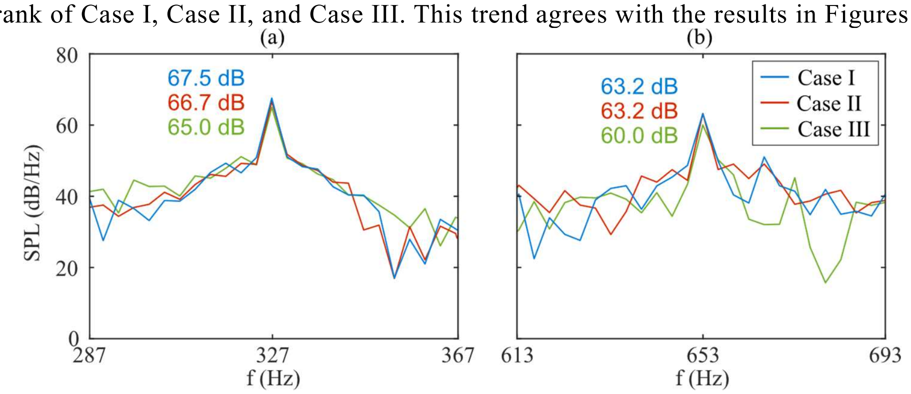

Figure 7. The SPL of the sound pressure at the microphone M1 upstream of the fan. The tonal frequency

a) $BPF = 327$ Hz, b) $BPF_1 = 653$ Hz. The SPL values of the tones are presented.

### 5.4 Spectral analysis of tonal noise sources

The results of the surface pressure fluctuations at the $BPF$ are illustrated for the three cases in Figure 8. The location of the highest surface pressure fluctuation is at the same position (the BLE close to the shroud) for all cases. The differences are the magnitude and area with high magnitudes. In response to the effect that Case I and Case II have the largest sound pressure (see Figure 7), the two cases also have the largest area and magnitude for the tonal frequency. The high energy locations are consistent with the surface pressure fluctuations indicated in Figure 5. As discussed above, the high energy is caused by the interaction between the inlet-gap turbulence and the BLE (5).

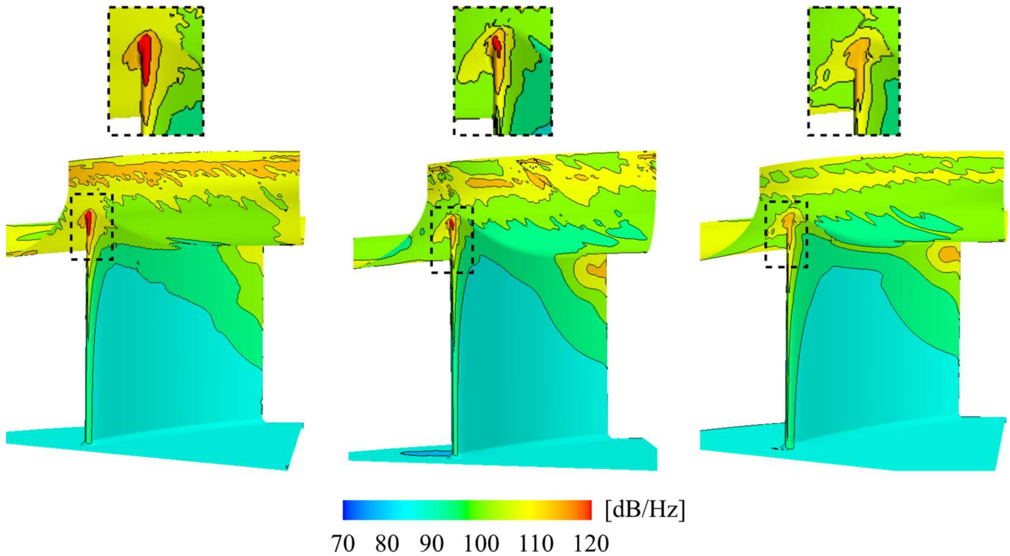


Figure 8. The SPL of surface pressure fluctuations at $BPF$ (327 Hz). From left to right: Case I, Case II, and Case III.

## 6. Conclusion

MVGs are designed to control the turbulence from the inlet gap of voluteless centrifugal fans, which are often utilized in HVAC systems. This new design concept is proposed for the purpose of reducing the tonal noise generation. A standard fan from the previous study (5) is taken as the reference (termed Case I in this paper), which is not installed with MVGs. The designed MVGs are assembled onto the reference fan using two arrangements: 14 MVGs evenly positioned on the shroud along the circumferential direction and near the inlet clearance (termed Case II), and 7 ones on the blade leading edge near the joint connection of the blade and shroud (termed Case III). These three cases are compared for their aerodynamic and aeroacoustic characteristics. The idea of designing MVGs is motivated by the findings in a previous study by the present authors, where the gap flow was addressed as an dominant source of the tonal noise. The flow is simulated using a hybrid method coupling the IDDES with Formulation 1A of Farassat.

The comparison of the three fans, Cases I–III, shows that adding MVG reduces the pressure rise downstream of the fan but increases the torque. Case II with 14 MVGs near the inlet gap has better fan performance than Case III with 7 MVGs at the BLE.

The three cases present a similar trend for the RMS pressure, from the inlet to the middle span of the blade, i.e., the middle of the flow passage. The RMS pressure is largest near the inlet, and decays as the distance to the inlet gap increases. Case I and III have their lowest values at the backplate. In contrast, Case II has its smallest value at the middle and as the distance to the gap grows the RMS pressure increases. Compared to the other cases, Case III overall has lower RMS amplitudes in the flow passage.

High vorticity magnitudes are found near the shroud and BLE surfaces for all three fans. As the distance to the inlet gap and the shroud increases, the total area of the regions with high vorticity magnitudes decreases. Moreover, the areas of the three fans decrease in the order of Case I, Case II, and Case III. It means that the MVGs are effect to reduce the turbulence, especially for the 7 MVG arrangement near the BLE.

By adding MVG, the aerodynamic and acoustic performances are affected with opposite trends. The assembling of the MVGs to the BLE (Case III) leads to the higher reduction in generating the tonal noise at $BPF$ and its first harmonic frequency, $BPF_1$. However, this worsens the aerodynamic performance for Case III


## ACKNOWLEDGEMENTS

Swegon Operation finances the present work. The simulations were performed on resources provided by the Swedish National Infrastructure for Computing (SNIC) at C3SE.


## REFERENCES


1. Berglund B, Lindvall T, Schwela D. New guidelines for community noise. Noise Vib. Worldwide, 2000; 31:24-29.
2. Azimi M. Noise reduction in building using sound absorbing materials. J. Archit. Eng. Technol. 2017.
3. Wolfram D, Carolus T.H. Experimental and numerical investigation of the unsteady flow field and tone generation in an isolated centrifugal fan impeller. Journal of Sound and Vibrations, 2010; 329:4380-4397.
4. Sanjose M, Moreau S. Direct noise prediction and control of an installed large low-speed radial fan. European Journal of Mechanics, 2017; 61:235-243.
5. Ottersten M, Yao H.-D, Davidson L. Tonal noise of voluteless centrifugal fan generated by turbulence stemming from upstream inlet gap. Phys. Fluids, 2021; 33,. https://doi.org/10.1063/5.0055242
6. Che B, Chu N, Schmidt S.J, Cao L, Likhachev D, Wu D. Control effect of micro vortex generators on leading edge of attached cavitation. Phys. Fluids, 2019; 31.
7. Gang L, Zhengtao Z, Pingguo Z. Numerical study on noise reduction of wind turbine blade vortex generators. Conf. Ser.: Earth Environ. Sci 2019; 358.
8. Shur M.L, Spalart P.R, Strelets M.K, Travin A.K. A Hybrid RANS-LES Approach with Delayed-DES and Wall-Modelled LES Capabilities. International J. Heat and Fluid Flow, 2008; 29:1638-1649.
9. Ffowcs Williams J.E, Hawkings D.L. Theory relating to the noise of rotating machinery. Journal of Sound and Vibration, 1969; 10:10-21.
10. Siemens PLM Software STAR-CCM+ User Guide. Version 12.04, 2017.
11. Salunkhe S, Fajri O.E, Bhushane S, Thompson D, O´Dohety D, O´Dohety T, Mason-Jones A. Validation of tidal stream turbine wake predictions and analysis of wake recovery mechanism. Journal of Marine Science and Engineering, 2019; 7.
12. Rynell A, Efraimsson G, Chevalier M, Åbom M. Inclusion of upstream turbulent inflow statistics to numerically acquire proper fan noise characteristics. SAE Technical Paper 2016-01-1811, 2016.
13. Rynell A, Chevalier M, Åbom M, Efraimsson G. A numerical study of noise characteristics originating from a shrouded subsonic automotive fan. Applied Acoustics 2018; 140:110-121.
14. Brentner K.S, Farassat F. Analytical comparison of the acoustic analogy and Kirchhoff formulation for moving surfaces. AIAAA J 1998; 36:1379-86.
15. Neise W. Review of fan noise generation mechanisms and control methods. In: Proceedings of the Fan Noise 1992 International Symposium, Senlis, France. 1992; 45-56.
16, Ottersten M, Yao H.-D, Davidson L. Unsteady Simulation of tonal noise from isolated centrifugal fan. Proceedings of Fan Noise 2018 Symposium, Darmstadt 2018.
17. Baris O, Mendonça F. Automotive turbocharger compressor CFD and extension towards incorporating installation effects. Proceedings of the ASME Turbo Expo 2011: Power for Land, Sea and Air, 2011.
18. Yao H.-D, Davidson L, Eriksson L.E. Surface integral analogy approaches for predicting noise from 3D high-lift low-noise wings. Acta Mech. Sin. 2014; 30:326-338.